THE JOURNAL OF BIOLOGICAL CHEMISTRY VOL. 286, NO. 6, pp. 4871–4881, February 11, 2011


# The T Cell Receptor β-Chain Second Complementarity Determining Region Loop (CDR2β) Governs T Cell Activation and Vβ Specificity by Bacterial Superantigens*[S]

Received for publication, September 27, 2010, and in revised form, November 5, 2010 Published, JBC Papers in Press, December 2, 2010, DOI 10.1074/jbc.M110.189068

**A. K. M. Nur-ur Rahman[‡§], Daniel A. Bonsor[¶], Christine A. Herfst[‡‖], Fraser Pollard[‡], Michael Peirce[‡], Aaron W. Wyatt[‡†], Katherine J. Kasper[‡], Joaquín Madrenas[‡§**1], Eric J. Sundberg[¶], and John K. McCormick[‡§‖2]**

*From the [‡]Department of Microbiology and Immunology and the [§]Centre for Human Immunology, The University of Western Ontario, London, Ontario N6A 5C1, Canada, the [¶]Boston Biomedical Research Institute, Watertown, Massachusetts 02472, the [‖]Lawson Health Research Institute, St. Joseph's Health Care, London, Ontario N6A 4V2, Canada, and **Robarts Research Institute, The University of Western Ontario, London, Ontario N6A 5K8, Canada*

**Superantigens (SAgs) are microbial toxins defined by their ability to activate T lymphocytes in a T cell receptor (TCR) β-chain variable domain (Vβ)-specific manner. Although existing structural information indicates that diverse bacterial SAgs all uniformly engage the Vβ second complementarity determining region (CDR2β) loop, the molecular rules that dictate SAg-mediated T cell activation and Vβ specificity are not fully understood. Herein we report the crystal structure of human Vβ2.1 (hVβ2.1) in complex with the toxic shock syndrome toxin-1 (TSST-1) SAg, and mutagenesis of hVβ2.1 indicates that the non-canonical length of CDR2β is a critical determinant for recognition by TSST-1 as well as the distantly related SAg streptococcal pyrogenic exotoxin C. Frame work (FR) region 3 is uniquely critical for TSST-1 function explaining the fine Vβ-specificity exhibited by this SAg. Furthermore, domain swapping experiments with SAgs, which use distinct domains to engage both CDR2β and FR3/4β revealed that the CDR2β contacts dictate T lymphocyte Vβ-specificity. These findings demonstrate that the TCR CDR2β loop is the critical determinant for functional recognition and Vβ-specificity by diverse bacterial SAgs.**

Antigen-specific T cell-mediated immunity is initiated through the interaction of the αβ T cell receptor (TCR)[3] with a processed peptide antigen presented within the distal groove of self major histocompatibility (pMHC) complexes. A general consensus for typical TCR-pMHC recognition is that germ line encoded complementarity determining region loops (CDR) 1 and CDR2 of both the TCR α- and β-chains primarily recognize the α-helices of self pMHC complexes, while peptide specificity is mainly driven by the CDR3 loops (1, 2).

Bacterial superantigens (SAgs) are potent immunostimulatory toxins that distort the molecular 'rules' which dictate normal TCR-pMHC class II (pMHC II) interactions. SAgs function by binding to lateral surfaces on both TCR β-chain variable domains (Vβ) (3) and pMHC II complexes (4), resulting in the activation of T cells in a Vβ-restricted manner (5). In the standard TCR-SAg-pMHC II model, the TCR β-chain, and pMHC II α-chain are wedged apart by the SAg such that the CDR3 loops of the αβ TCR cannot interact directly with the antigenic peptide contained within the pMHC II complexes (6). Because SAgs bind the germ line encoded Vβ region, while essentially ignoring the highly diverse CDR3β loop, the frequency of T cells responding to SAg exposure exceeds that of conventional peptide antigens by many orders of magnitude. Through this mechanism, SAgs may ultimately mediate a cytokine storm disease known as the toxic shock syndrome (7).

The bacterial pathogens *Staphylococcus aureus* and *Streptococcus pyogenes* are each capable of producing multiple distinct bacterial SAgs that fall into at least five distinct evolutionary groups, designated as I through V (Fig. 1*A*) (7, 8), that share a conserved three-dimensional fold (9) (Fig. 1*B*). Despite this conserved structure, SAgs can bind to pMHC II through diverse mechanisms (10–16). In terms of TCR recognition, all characterized SAgs interact with the apical portion of the TCR β-chain, but this occurs with distinct geometries (6, 17–21) (Fig. 1*B*). For example, the Group I SAg toxic shock syndrome toxin-1 (TSST-1) binds to CDR2β and FR3β (20); Group II SAgs such as staphylococcal enterotoxin (SE) B, SEC3 and streptococcal pyrogenic exotoxin (Spe) A bind pri-

* This work was supported, in whole or in part, by National Institutes of Health Grant AI065690 (to E. J. S.) and a Canadian Institutes of Health Research (CIHR) operating grant (to J. K. M.). Stipend support (to A. K. M. N. R.) was provided in part by scholarships from the Schulich School of Medicine and Dentistry and from an Early Research Award from The Ontario Ministry of Research and Innovation. Laboratory infrastructure was supported by a New Opportunities Fund award from the Canadian Foundation for Innovation and the Ontario Innovation Trust (to J. K. M.).

[S] The on-line version of this article (available at http://www.jbc.org) contains supplemental Tables S1–S3.

† This study is dedicated to the memory of Aaron William James Wyatt (1983–2008), friend and colleague.

*The atomic coordinates and structure factors (code 3MFG) have been deposited in the Protein Data Bank, Research Collaboratory for Structural Bioinformatics, Rutgers University, New Brunswick, NJ (http://www.rcsb.org/).*

[1] Holds a Tier I Canada Research Chair in Immunobiology.

[2] Holds a New Investigator award from the CIHR. To whom correspondence should be addressed. Tel.: 519-661-3409; Fax: 519-661-3499; E-mail: john.mccormick@schulich.uwo.ca.

[3] The abbreviations used are: TCR, T cell receptor; CDR, complementarity determining region; FR, framework region; HV, hypervariable region; MHC, major histocompatibililty complex; MAM, *Mycoplasma arthritidis* mitogen; PBMCs, peripheral blood mononuclear cells; pMHC, peptide-MHC; SAg, superantigen; SE, staphylococcal enterotoxin; Spe, streptococcal pyrogenic exotoxin; TEV, tobacco etch virus; TSST-1, toxic shock syndrome toxin-1; Vβ, variable region of the T cell receptor β chain.

marily to CDR2β, FR3β, and HV4β (6, 19, 21); the Group IV SAg SpeC binds to CDR1β, CDR2β, CDR3β, and HV4β (21); and the Group V SAg SEK binds to CDR2β, FR3β, and FR4β (18). Although the Vβ binding site for the *Mycoplasma arthritidis* mitogen (MAM) nearly overlaps with that of SEB, MAM represents a structurally and phylogenetically distinct SAg that also interacts directly with Vα (22). Taken together, the one common feature for all of the structurally characterized bacterial SAgs is that each engages the CDR2 loop of Vβ (Fig. 1*B*), yet the broad functional relevance of CDR2β for this large family of toxins is still unknown.

The TSST-1 and SpeC SAgs are two distantly related SAgs, both of which are highly specific for T cells bearing the human Vβ2 (hVβ2) TCR, but structural studies indicate that the binding footprints for this common ligand are distinct (20, 21). Human Vβ2 is somewhat unique as this β-chain contains insertions on its amino acid backbone that are lacking in other human β-chains. These insertions include $Phe^{27a}$ in CDR1β found uniquely in hVβ2, and $Ser^{52a}$ in CDR2β and $Tyr^{56}$ in FR3β found only in hVβ2 and hVβ4. The presence of $Phe^{27a}$ and $Ser^{52a}$ result in longer than typical CDR1β and CDR2β loops with non-canonical structures. Therefore, the restrictive Vβ profiles of TSST-1 and SpeC are thought to be due to peculiar Vβ amino acid insertions. More promiscuous SAgs, however, such as SEB, that exhibit a broader range of Vβ targets interact primarily with main-chain atoms of Vβ chains, are thought to recognize Vβs predominantly through a conformational-dependent mechanism (reviewed in Ref. 9).

Within protein-protein interfaces, subsets of the interfacial residues that contribute disproportionately to the overall affinity of the interaction are termed hot spots, and discrete clusters of hot spot residues are termed hot regions (23, 24). Biochemical evidence indicates that TSST-1 however, contains two distinct binding hot regions that target residues within CDR2β and FR3β, and these two hot regions exhibit positive binding cooperativity (25). Although SpeC engages all 3 CDRs as well as HV4β, this SAg contains a functional hot region including SpeC $Tyr^{15}$ and SpeC $Arg^{181}$ that primarily engages the hVβ2.1 $Ser^{52a}$ insertion of CDR2β (21, 26), providing an explanation as to why SpeC is largely specific for Vβs 2 and 4 (27), both of which contain the $Ser^{52a}$ insertion.

In this work, we sought to further unravel the molecular basis of SAg selectivity for TCR β-chains. Exhaustive mutational analysis of the wild-type hVβ2.1 chain expressed from human T cells indicates that the non-canonical length of the CDR2β loop is a critical factor for the functional engagement of both TSST-1 and SpeC, and a predicted hotspot within FR3β was also critical for TSST-1 function. Since all structurally characterized SAgs engage CDR2β (6, 18–21) (Fig. 1), we hypothesized that the CDR2β loop was a key determinant for Vβ discrimination, which is the hallmark activity of SAgs (28). To test this, we created domain swapping mutations between the Group V SAgs staphylococcal enterotoxin K (SEK) and streptococcal pyrogenic exotoxin I (SpeI), which contain distinct SAg domains that interact exclusively with either CDR2β or the FR3β/FR4β regions (8, 18). Analysis of Vβ expansion by these hybrid SAgs establishes that the CDR2β loop is the critical determinant for dictating Vβ specificity.

## EXPERIMENTAL PROCEDURES

*Crystallization, Data Collection, Structure Determination, and Refinement*—TSST-1 and hVβ2.1 proteins were produced and purified as described previously (20, 25). A 1:1 TSST-1/hVβ2.1 complex was prepared by mixing the two components together, with hVβ2.1 in slight excess (molar ratio of 1:1.2, respectively), followed by purification on a Superdex S200 10/300 column (GE Healthcare) equilibrated in 50 mM Tris, 25 mM sodium chloride, pH 7.5. The purified TSST-1/hVβ2.1 complex was concentrated to 6.3 mg $ml^{-1}$. Crystals were obtained by hanging drop vapor diffusion, where 1 μl of complex was mixed with 1 μl of the reservoir solution composed of 22% polyethylene glycol 8000 and 0.46 M lithium sulfate. Crystals were flashed cooled in mother liquor containing 20% glycerol. A data set was collected at the National Synchrotron Light Source, Brookhaven National Laboratory, beam line X6A at 100 K. The data were reduced with iMOSFLM and SCALA in the CCP4 suite of programs (CCP4, 1994). The structure was solved by molecular replacement using the program Phaser with the atomic coordinates of the complex between TSST-1 and the hVβ2.1 affinity-matured variant D10 (Ref. 20; PDB accession code 2IJ0) as a search model. The structure was refined using REFMAC and model building performed using Coot. Coordinates have been deposited in the Protein Data Bank with the accession code 3MFG.

*Cloning Procedures*—Standard DNA manipulations were performed as described (29) using enzymes supplied from New England Biolabs (Pickering, Ontario) in accordance with the manufacturer's instructions. Oligonucleotides were obtained from Sigma Genosys (Burlington, Ontario). PCRs were performed in a Peltier Thermocycler (MJ Research, Miami, FL) with *Vent* DNA polymerase (Invitrogen) and PCR products were purified using the QIAquick PCR purification kit (Qiagen Inc., Mississauga, ON). All cloned PCR products were sequenced in their entirety at the Robarts Research Institute Sequencing Facility (London, Ontario, Canada) to ensure correct mutations and PCR fidelity. *Escherichia coli* XL1-blue and BL21(DE3) was cultured aerobically in Luria Bertani broth (Difco Laboratories Inc, Detroit, MI) at 37 °C, and solid media was obtained by the addition of 1.5% (w/v) Bacto-agar (Difco). Kanamycin (50 μg/ml) was used as selective agent as required. All reagents were made with water purified through a Milli-Q water purification system (Millipore, Mississauga, ON).

*Construction of Wild-type and Mutant hVβ2.1 vectors*—The full-length wild-type hVβ2.1 cDNA (26) was directionally subcloned into the KpnI and BamHI sites of the expression vector pMAX (Amaxa). The various hVβ2.1 mutant constructs were generated using an overlapping megaprimer PCR method using the oligonucleotides listed in supplemental Table S1. All hVβ2.1 mutations were verified by sequencing both strands.

*Construction of hVβ2.1-expressing HuT78 T Cells and Activation Measurements*—To generate functional epitopes of SpeC and TSST-1 on the surface of hVβ2.1, the HuT78 T cell line (30) was used to express hVβ2.1-chain conjugated to en-

dogenous hVα. 20 μg of pMAX vector harboring either wild-type or mutated hVβ2.1 constructs was electroporated into 8 million HuT78 T cells using 250 V and 250μF (Bio-Rad). HuT78 T cells transfected with pMAX::eGFP alone was used as negative control. Surface expression of hVβ2.1 paired with endogenous hVα was confirmed using FACS analysis with FITC-conjugated anti-Vβ2 antibody (eBioscience) (data not shown). Anti-Vβ2 antibody and anti-CD28 antibody were coupled onto beads (Dynabeads® M-450 Tosylactivated, Invitrogen) as per the manufacturer's instruction. The final preparation of anti-Vβ2/anti-CD28 beads were resuspended in complete R-10 media. 24 h after electroporation, transfected HuT78 T cells were counted, and 200,000 cells were incubated with SpeC or TSST-1 at 1 μg/ml, or anti-Vβ2/anti-CD28 beads at one bead per transfected HuT78 T cell for 18 h in 5% $CO_2$ at 37 °C. Activation was monitored using IL-2 ELISA (eBioscience).

*Superantigens*—Cloning of the wild-type genes for SpeC, TSST-1, SpeI and SEK has been described (8, 18, 25, 26). Mutagenesis was conducted using megaprimer-PCR designed to introduce domain-swapping mutants between SpeI and SEK using oligonucleotides listed in supplemental Table S2. Recombinant SAgs were produced by overexpression from *E. coli* BL21(DE3) with N-terminal $His_6$ tags, purified by nickel affinity chelation chromatography, and $His_6$ tags were removed by cleavage of an engineered tobacco etch virus (TEV) protease cleavage site using autoinactivation resistant $His_6$::TEV protease, as described (8, 18). All recombinant SAgs ran as discrete homogenous bands by SDS-PAGE.

*Primary Cells and Quantitative Real-time PCR*—Experiments using human lymphocytes were reviewed and approved by The University of Western Ontario Research Ethics Board for Health Sciences Research Involving Human Subjects. Ficoll gradient purified human PBMCs were stimulated *ex vivo* in 24-well microtiter plates ($1 \times 10^6$ cells/well) in R10 media (26) with the various SEK or SpeI wild-type or hybrid proteins at 1 μg/ml, in triplicate. Cells were incubated in 5% $CO_2$ at 37 °C for 4 days. Afterward cells were harvested and total RNA prepared using RNeasy Spin columns (Qiagen). RNA (500 ng) was reverse transcribed using Superscript II (Invitrogen), and qPCR was performed on cDNA using a specific forward primer for hVβ5, hVβ6.7, hVβ9, an hVβ21.3, coupled with a reverse Cβ transcript specific primer. qPCR reactions were performed using SybrGreen chemistry (Bio-Rad) on a Rotogene 6000 instrument, and the Vβ specific transcript levels were normalized to a Cβ1/Cβ2 transcript primer pair as a measure of total TCR β-chain expression using oligonucleotides listed in supplemental Table S3.

*Statistics*—Results are represented as the mean ± S.E. where statistical significance between two conditions was determined by the Student's *t* test using Prism 4.0 (GraphPad Software).

## RESULTS AND DISCUSSION

*Crystal Structure of Wild-type hVβ2.1-TSST-1 Complex*—TSST-1 is unique among the SAg toxin family and is classified as the only Group I SAg (Fig. 1*A*). TSST-1 is believed to be responsible for essentially all cases of the menstrual-associated TSS cases, and many non-menstrual TSS cases (7). It seems counterintuitive that TSST-1, while likely the most clinically significant bacterial SAg, is also one of the most Vβ specific, being exclusive for hVβ2-expressing T cells (31).

Previous work using yeast display of hVβ2.1 coupled with affinity maturation experiments identified and characterized a number of high-affinity hVβ2.1 variants that bound TSST-1 with increasing affinities up to 12,800-fold for the D10 variant (25, 32). The D10 variant was subsequently used to solve the co-crystal structure with wild-type TSST-1, and modeling of the wild-type hVβ2.1 onto this complex revealed the structural basis for how TSST-1 engages the human hVβ2 TCR (20). Here we report the crystal structure of TSST-1 in complex with the wild-type version of hVβ2.1 called Ep8, previously used for stabilization on the surface of yeast. The amino acid sequence of Ep8 is identical to naturally occurring hVβ2.1 except for two mutations (A13V and S88G) that would fall into the Vβ:Cβ interface and allowed for stabilized expression on yeast, but the mutations do not occur within the TSST-1 interface (32). The TSST-1/hVβ2.1 crystal structure was refined to 2.3 Å resolution. Data collection and refinement statistics are shown in Table 1.

*Functional Epitope Mapping on the Surface of the hVβ2.1 TCR for TSST-1 and SpeC*—From prior co-crystallization studies (12, 16, 20, 21), and using the wild-type hVβ2-TSST complex solved here, coupled with corroborating mutagenesis data (11, 26, 33–35), supramolecular T cell activation complexes can be modeled for both TSST-1 and SpeC (Fig. 2). For comparison, a typical TCR-pMHC complex of conventional antigen recognition, where the CDR3 loops from both α- and β-chains center on the antigenic peptide is shown in Fig. 2*A* (36). For TSST-1 (Fig. 2*B*) and SpeC (Fig. 2*C*), both SAgs engage the TCR Vβ and pMHC II molecules using lateral surfaces, forming a bridge (*e.g.* TSST-1) or a wedge (*e.g.* SpeC) between the two immune receptors. In both cases, the SAg displaces the CDR3 loops away from the antigenic peptide preventing peptide recognition by the TCR, while SpeC contains an additional high-affinity, zinc-dependent MHC II interaction (16, 34).

Crystallographic analysis for TSST-1 and SpeC provides us with the molecular contacts required for SAg engagement of hVβ2, as well as the plasticity of the SAg binding interface on the surface of this common ligand (Fig. 2, *D* and *E*). Although the wild-type Ep8-TSST-1 complex is essentially identical in orientation to the high-affinity D10-TSST complex (20), it is radically different from the other characterized SAg-Vβ structures (Fig. 1*B*). TSST-1 binds more laterally to the apical region of Vβ, interacting with a contiguous segment of residues stretching from $Gly^{51}$ to $Lys^{64}$ comprising the CDR2β loop and FR3β region of hVβ2.1 (Fig. 2*D*). The engagement of hVβ2.1 by SpeC is more similar to other characterized SAgs, except SpeC binds in a slightly altered orientation with a larger binding interface engaging residues from all three CDRβ loops and HV4β, which coalesce into a distinct binding region on the surface of hVβ2.1 (Fig. 2*E*) (21).

To understand the molecular requirements for hVβ2 selectivity and activation by TSST-1 and SpeC, 24 surface residues in the wild-type hVβ2.1 involved in binding these SAgs were

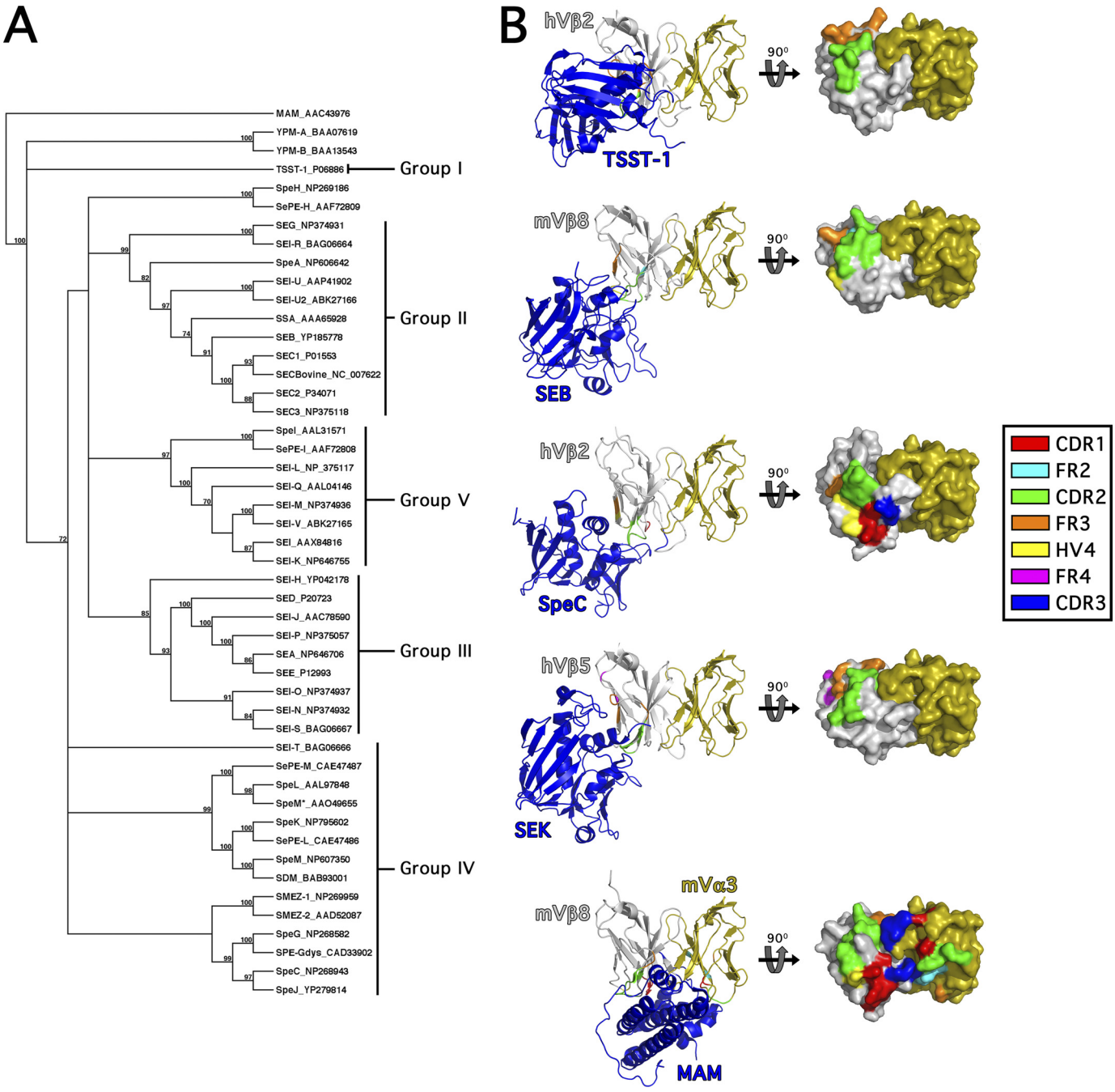


FIGURE 1. **Phylogenetic relationships and representative Vβ-binding topologies for the bacterial SAgs.** *A*, phylogenetic tree of known bacterial SAgs. The unrooted tree was based on the alignment of amino acid sequences using Clustal W (47) and constructed with the unweighted pair group method using arithmetic averages (UPGMA) in MacVector 7.2.3. The SAg abbreviations are indicated followed by the relevant accession number. As previously proposed (7), the five main groups of SAgs belonging to the pyrogenic toxin class are indicated. MAM, YPM, and non-Group A streptococcal SAgs are also included in the analysis. The number of times each branch was supported from 1000 bootstraps is shown as a percentage. *B*, overview of SAg engagement of the T cell receptor Vβ domain. *Ribbon diagrams* (*left panel*) of the TSST-1-Vβ2.1, SEB-Vβ8.2 (19), SpeC-Vβ2.1 (21), SEK-Vβ5 (18), and MAM-Vβ8.2/Vα3 (22) complexes. The Vβ domains (in *gray*) are aligned to one another to highlight the distinct regions of the apical side of the Vβ domains engaged by these SAgs, and the mouse Vα3 (mVα3) (in *orange*) from the MAM-Vβ8.2/Vα3 structure is modeled onto the other structures for comparison. Surface-filled models (*right panel*) of the corresponding Vβ domains with the molecular surface buried by the corresponding SAgs are demarcated. CDR, HV, and FR regions buried in the interface by the corresponding SAg are color-coded as indicated in the legend.

targeted for alanine-scanning mutagenesis (Fig. 2, *D* and *E*). Three naturally occurring alanines present in hVβ2.1 ($Ala^{29}$, $Ala^{54}$, and $Ala^{96}$) were instead replaced with both glycine and valine. In addition, three deletion mutants were generated including the non-canonical insertions $Phe^{27a}$ and $Ser^{52a}$ in CDR1β and CDR2β loops, respectively (21), as well as the unique insertion $Tyr^{56}$ in FR3β (25). The non-canonical CDR2β insertion $Ser^{52a}$ was also mutated to Cys (S52aC), as some naturally occurring hVβ2 alleles carry Cys at this position, and to Gly (S52aG), to remove the interacting side-chain and to introduce more flexibility, yet maintain the length of the CDR2β loop. In total, 31 hVβ2.1 mutants were generated

**TABLE 1**
**Summary of crystallographic analysis for the TSST-1/Vβ2.1 complex**

| | |
|---|---|
| **Data collection** | |
| Space group | I 4 2 2 |
| **Cell dimensions** | |
| a, b, c (Å) | 242.62, 242.62, 47.14 |
| α, β, γ (°) | 90.0, 90.0, 90.0 |
| Resolution (Å)[a] | 47.6-2.37 (2.5-2.37) |
| $R_{sym}$[a,b] | 13.4 (99.9) |
| I/σI[a] | 15.5 (2.5) |
| Completeness (%)[a] | 99.9 (99.4) |
| Redundancy[a] | 14.9 (11.2) |
| **Refinement** | |
| Resolution (Å) | 47.6-2.37 Å |
| No. reflections | 28972 |
| $R_{work}/R_{free}$[c] | 23.4/28.3 |
| **B factors (Å²)**[d] | |
| TSST-1 | 31.9 |
| hVβ2.1 | 33.8 |
| Water | 30.6 |
| **RMS deviations**[e] | |
| Bond lengths (Å) | 0.023 |
| Bond angles (°) | 1.91 |

[a] Numbers in parentheses correspond to the highest resolution shell.
[b] $R_{sym} = \Sigma\Sigma|I_{i,j} - <Ij>|/\Sigma\Sigma I_{i,j}$.
[c] $R_{work} = \Sigma_{hk}||F_o| - k|F_c||/\Sigma hk|F_o|$; $R_{free}$, same for a test set of 5% reflections not used during refinement.
[d] Average B factors.
[e] Root-mean-square deviation given from ideal values.

to elucidate the molecular basis of selectivity and activation of hVβ2-expressing T cell by both TSST-1 and SpeC.

Wild-type hVβ2.1 was transfected into HuT78 T cells (37) and stimulated with titrations of TSST-1 or SpeC (Fig. 3*A*). HuT78 T cells naturally express endogenous hVβ23, which is an irrelevant Vβ for the SAgs used in this work, and thus the hVβ2.1-chain paired with the endogenous Vα-chain. HuT78 T cells also express endogenous HLA-DR4 molecules (38), which can cross-present TSST-1 or SpeC to neighboring HuT78 T cells. Using this system, both TSST-1 and SpeC were able to activate these cells in a dose-dependent manner (Fig. 3*A*).

To map the functional epitopes of TSST-1 and SpeC on the surface of hVβ2.1, each hVβ2.1 mutant was transfected into HuT78 T cells and stimulated with either wild-type TSST-1 or SpeC at 1 μg/ml (Fig. 3, *B–F*). To control for transfection efficiencies and TCR expression, each transfection was also stimulated with anti-Vβ2/anti-CD28 (α-Vβ2/α-CD28) beads, at one bead per T cell. The IL-2 levels from controls lacking SAg, and the TSST-1 and SpeC stimulations, were normalized to the α-Vβ2/α-CD28 beads response which was set at 100%. For 5 of the hVβ2.1 mutations (K53A, A54V, K62A, D63A, and K64A), IL-2 produced from these transfections stimulated with the α-Vβ2/α-CD28 beads was severely compromised, possibly due to disruption of the α-Vβ2 binding epitope. The IL-2 responses of mutant K53A was therefore normalized to that of the wild-type hVβ2.1 transfections, and since A54G could be stimulated with α-Vβ2/α-CD28 (Fig. 3*C*), the A54V data were discarded. As SpeC does not engage FR3β residues, the IL-2 responses from FR3β mutants K62A, D63A, and K64A were normalized to that of SpeC-stimulated HuT78 T cells transfected with wild-type hVβ2.1 (Fig. 3*F*). Lastly, functional forms of the $Tyr^{56}$ deletion, or the Y56A mutation, could not be detected on the surface of HuT78 T cells by flow cytometry and thus these mutants could not be evaluated.

*The Molecular Basis of hVβ2.1 Recognition by TSST-1*—TSST-1 interacts with fifteen contiguous residues including $Glu^{51}$ through $Thr^{55}$ in CDR2β, and continuing into the FR3β region from residues $Tyr^{56}$ to $Lys^{64}$ (Fig. 2*D*). Within CDR2β, E51A, G52A, and K53A each showed moderately impaired IL-2 responses to TSST-1 and these phenotypes were consistent with residues identified from the generation of the high-affinity TSST-1 binding hVβ2.1 variants previously described (32). Two well studied high-affinity hVβ2.1 variants named C10 and D10 contain 10 and 14 mutations relative to the yeast stabilized wild-type Ep8, with ~6,800-fold ($K_D$ = 340 pM) and ~13,000-fold ($K_D$ = 180 pM) stronger affinities for TSST-1, respectively, relative to Ep8 ($K_D$ = 0.6 μM) (25, 32). In C10, mutagenesis of only three of the affinity-matured residues ($Phe^{52a}$, $Asn^{53}$, $Val^{61}$) to alanine demonstrated faster off-rates than C10 (32) and only 4 affinity-matured residues within D10 ($Glu^{51}$, $Phe^{52a}$, $Lys^{53}$, and $Val^{61}$) when mutated back to the wild-type residues showed significant changes in affinity (25, 32). Consistent with our findings, each of these residues (other than $Ser^{52a}$ discussed below) showed reduced responses in the wild-type hVβ2.1 backbone providing biological significance to the prior biochemical analysis. In the wild-type Ep8-TSST-1 structure there are no direct contacts of $Ser^{52a}$ with TSST-1 and the Ser52a → Ala mutation retained wild-type function (Fig. 3*C*), but from the affinity maturation experiments with D10, $Ser^{52a}$ → Phe was demonstrated to dramatically increase the affinity of this interaction (25, 32). To further evaluate if $Ser^{52a}$ itself was important, or if the non-canonical conformation of CDR2β was necessary for TSST-1 activation, three other mutations at $Ser^{52a}$ were assessed. S52aC and S52aG each demonstrated neutral profiles upon TSST-1 and α-Vβ2/α-CD28 beads stimulation. The most dramatic mutation however, was the deletion of $Ser^{52a}$, which abrogated IL-2 secretion by TSST-1 stimulation (Fig. 3*D*). The fact that TSST-1 could activate S52aG indicates that the presence of a specific side-chain at position 52a is not a requirement for efficient T cell activation by TSST-1.

Within the FR3β residues involved in the interaction with TSST-1, E61A had a moderate phenotype, and K62A was a critical mutation (Fig. 3*F*). The E61V mutation was also identified in the D10 affinity maturation pathway following a likely random PCR error, and the subsequent Val → Ala mutation within the C10 variant demonstrated faster off-rate kinetics compared with C10 (32). In the wild-type hVβ2-TSST structure, $Lys^{62}$ hydrogen bonds with both TSST-1 residues $Glu^{132}$ and $His^{135}$, each of which are individually critical for TSST-1 function (33). Although $Lys^{62}$ was not identified through the affinity maturation experiments, mutation to Ala at this position in C10 also demonstrated faster off-rate kinetics (32). Based only on CDR2β sequences, TSST-1 would be expected to activate T cells expressing hVβ4; however, hVβ4 alleles contain an Ile at position 62 in FR3, explaining how TSST-1 shows such fine specificity for hVβ2-expressing T cells.

As TSST-1 makes only main chain contacts with hVβ2.1 residues $Glu^{57}$ and $Val^{60}$, these two residues were not subjected to mutagenesis, and the contribution of $Tyr^{56}$ could not

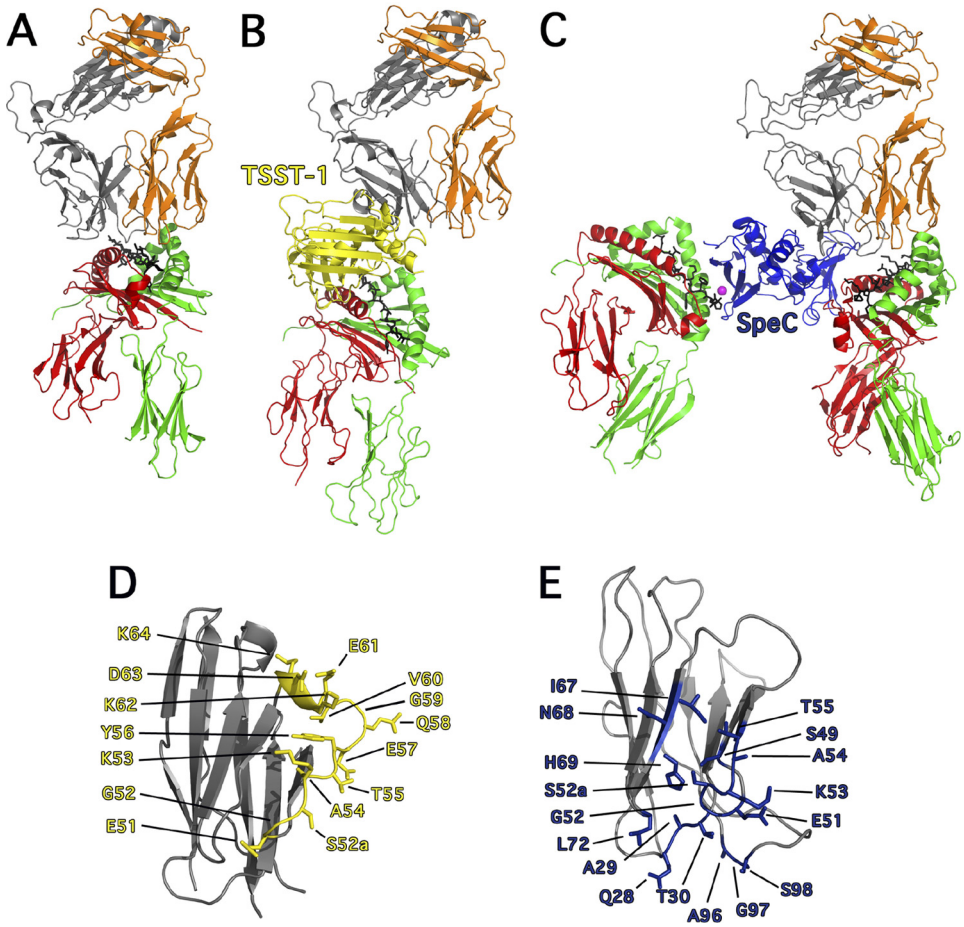


FIGURE 2. **Exposition of the differences between conventional TCR-pMHC and TCR-SAg-pMHC T cell signaling complexes.** *A*, cartoon representation of conventional TCR-pMHC ternary complex (36), where the TCR adopts a semi-conserved diagonal docking mode on pMHC II. By and large, the CDR1 and CDR2 loops engage the α-helices of MHC II and the CDR3 loops engage the antigenic peptide. *B*, cartoon representation of the TSST-1-mediated T cell activation complex (20), where TSST-1 acts a bridge between TCR and pMHC II complex and direct TCR contact with pMHC II is abrogated, thus removing antigenic peptide recognition. *C*, cartoon representation of the SpeC-mediated T cell activation complex (11, 16, 21) where SpeC cross-links MHC II molecules through zinc-mediated, high-affinity binding to the pMHC II β-chain (*left*) (16), and as a wedge, by binding to the low-affinity binding site on the pMHC II α-chain (11) and preventing direct contacts between TCR Vβ and the antigenic peptide. Colors are as follows: MHC α-chain, *green*; MHC β-chain, *red*; antigenic peptide, *black*; TCR α-chain, *orange*; TCR β-chain, *gray*; $Zn^{2+}$ ion, *magenta*; TSST-1, *yellow* and SpeC, *blue*. *D*, close up view of hVβ2.1 (PDB code 3MFG) showing all the residues involved in binding to TSST-1. *E*, close up view of hVβ2.1 (PDB code 1KTK) showing all residues involved in binding to SpeC.

be assessed in this work because neither the $Tyr^{56}$ deletion nor T56A mutation was detectable on the surface of T cells (data not shown). Nevertheless, from mutational analysis in the C10 hVβ2.1 variant, C10 Y56A demonstrated an almost 200-fold reduction in affinity. $Tyr^{56}$ is located at the center of the c″ β-strand and forms many intramolecular contacts within hVβ2.1. This residue has been proposed to be important for linking the long-range cooperative binding regions for TSST-1 between CDR2β and FR3β (25) and although we could not assess the function in the current work, this particular residue is also deemed critical for TSST-1 recognition of hVβ2.1.

A few of the hVβ2.1 mutations demonstrated slight, but consistent, increases in IL-2 production and included T30A, I67A, and S98A. None of these residues make direct contacts with TSST-1, or are located in close proximity to the putative α-Vβ2 epitope, but in each case the corresponding IL-2 responses for SpeC were also marginally increased. As such we do not believe these increased responses reflect direct SAg-binding responses.

In the TSST-1-hVβ2.1 complex, there are six TSST-1 interacting residues in the interface that are known to be individually critical for the activation of $hV\beta2^+$ T cells ($Gly^{16}$, $Arg^{68}$, $Ser^{72}$, $Glu^{132}$, $His^{135}$, and $Gln^{139}$) (25, 33, 35). These residues form two distinct hot regions on the surface of TSST-1 surrounding CDR2β and FR3β of hVβ2.1 and are perfectly juxtaposed with the two hot-regions on hVβ2.1 identified here and from prior biochemical studies ($Glu^{51}$, $Gly^{52}$, $Lys^{53}$, $Tyr^{56}$, $Glu^{61}$, and $Lys^{62}$) (25, 32) (Fig. 4*A*). Thus the molecular basis of the extreme Vβ specificity for TSST-1 is a combination of both the non-canonical CDR2β conformation coupled with the hotspot residues on FR3β region, in particular the unique residues $Tyr^{56}$ and $Lys^{62}$.

*The Molecular Basis of SpeC Recognition by hVβ2.1*—The crystal structure of SpeC in complex with hVβ2.1 (21) demonstrates that SpeC interacts with three residues ($Gln^{28}$, $Ala^{29}$, and $Thr^{30}$) from CDR1β, seven residues ($Ser^{49}$, $Glu^{51}$, $Gly^{52}$, $Ser^{52a}$, $Lys^{53}$, $Ala^{54}$, and $Thr^{55}$) from CDR2β, four residues ($Ile^{67}$, $Asn^{68}$, $His^{69}$, and $Leu^{72}$) from HV4β and three residues ($Ala^{96}$, $Gly^{97}$, and $Ser^{98}$) from CDR3β. Based on IL-2

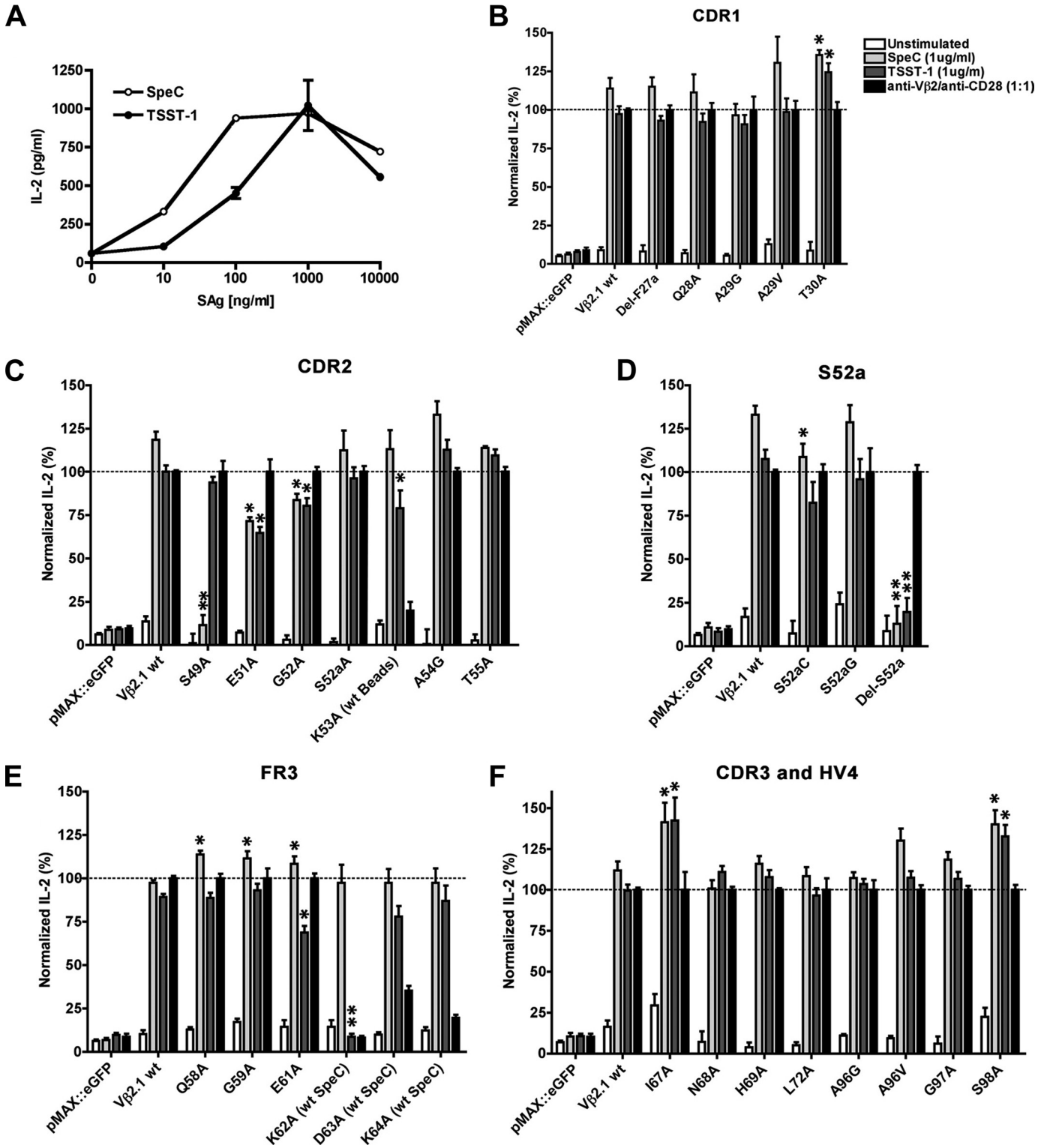


FIGURE 3. **Functional analysis of TSST-1 and SpeC binding interfaces on the hVβ2.1 TCR.** *A*, titration of TSST-1 and SpeC to optimize IL-2 secretion from HuT78-hVβ2.1 T cells. IL-2 secreted from electroporated HuT78 T cells transiently expressing hVβ2.1 mutations within CDR1 (*B*), CDR2 (*C*), $Ser^{52a}$ (*D*), and FR3 (*E*), and CDR3 and HV4 (*F*). For panels (*B–F*), electroporated HuT78 T cells expressing eGFP and wild-type hVβ2.1 were used as negative and positive controls, respectively, with SpeC and TSST-1 added at a final concentration of 1 μg/ml, and the internal control anti-Vβ2/anti-CD28 beads added at one bead per electroporated HuT78 T cells. Data shown are the average ± S.E. from at least three independent experiments each conducted in triplicate (*, $p < 0.05$ compared with HuT78-Vβ2.1, and **, $p < 0.05$ compared with HuT78 transfected with wild-type hVβ2.1 but not significantly different compared with HuT78 transfected with the eGFP negative control).

stimulation profiles for SpeC, residues within the CDR1β, HV4β, and CDR3β loops play no major individual role for the activation of $hV\beta2^+$ T cells (Fig. 3, *B* and *E*). The data for CDR1β was surprising as this loop is unique in that it contains an additional residue, $Phe^{27a}$, not present in the CDR1β loops from any of the other Vβ families. Although

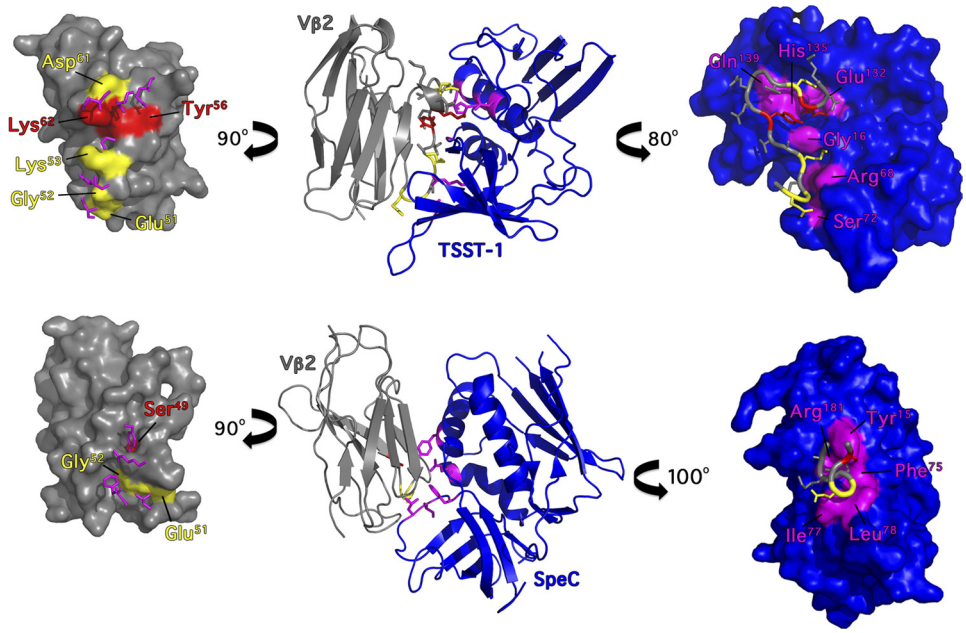


FIGURE 4. **Functional hotspots of TSST-1 and SpeC engage the CDR2β loop of hVβ2.1.** *Top*, TSST-1-hVβ2.1 complex. *Bottom*, SpeC-hVβ2.1 complex. The *middle panels* show ribbon diagrams of each SAg-Vβ complex, and the *left* and *right panels* show space-filling models for hVβ2.1, and TSST-1 or SpeC, respectively, rotated away from the central panel around the *y* axis as indicated. SAg residues critical for function are colored *magenta*. hVβ2.1 residues critical for function are colored *red*, and those with moderate phenotypes are colored *yellow*.

Phe$^{27a}$ does not interact directly with SpeC, this non-canonical insertion was deleted because this extra residue gives the hVβ2.1 CDR1β loop a non-canonical structure that projects toward SpeC (21). Furthermore, the presence of Phe$^{27a}$ in CDR1β has also been predicted to make hVβ2 more reactive to SpeC than hVβ4, which lacks Phe$^{27a}$, but has Ser$^{52a}$ in CDR2β loop. However, deletion of Phe$^{27a}$ had no impact on function (Fig. 3*B*).

Within CDR2β, mutating Ser$^{49}$ to alanine resulted in a significant phenotype, although this mutant was fully competent for activation by TSST-1 and α-Vβ2/α-CD28 beads (Fig. 3*C*). hVβ2.1 Ser$^{49}$ appears to function to anchor SpeC Tyr$^{15}$, a SpeC residue required for hVβ2.1 binding (26), allowing for the non-canonical CDR2β to engage the SpeC binding pocket. Despite the critical requirement for hVβ2.1 Ser$^{49}$, this residue is found in roughly one third of all human Vβs, and thus it does not likely contribute much in terms of fine Vβ-selectivity. CDR2β mutants E51A and G52A had moderate phenotypes (Fig. 3*C*). hVβ2.1 Glu$^{51}$ makes two van der Waals contacts with SpeC Ile$^{77}$, and hVβ2.1 Gly$^{52}$ makes two van der Waals interactions with SpeC Leu$^{78}$, and both these SpeC residues are known hot-spots on SpeC, although the G52A mutation may also affect the flexibility of CDR2β. The remainder of the CDR2β loop residues Lys$^{53}$, Ala$^{54}$, and Thr$^{55}$ had neutral phenotypes (Fig. 3*C*).

Previous work identified the $O_\gamma$ atom of Ser$^{52a}$ to be the focal point of several hydrogen bonds with SpeC residues (21, 26). Deletion of Ser$^{52a}$ abrogated IL-2 production from SpeC, yet SpeC was able to activate all of the various Ser$^{52a}$ point mutations, with only a slight reduction for S52aC (Fig. 3*D*). It was proposed that the $S_\gamma$ atom from the thiol group of Cys$^{52a}$, which occurs naturally in some hVβ2 alleles, could replace the $O_\gamma$ atom of Ser$^{52a}$ while maintaining hydrogen bonds with the interacting residues from SpeC (26). Although this may be the case, it was again surprising that S52aG was as efficient as either S52aA or S52aC for activation by SpeC.

Five SpeC residues within the SpeC-hVβ2.1 interface are each individually critical for the activation of hVβ2$^+$ T cells (11, 26). These residues (Tyr$^{15}$, Phe$^{75}$, Ile$^{77}$, Leu$^{78}$, and Arg$^{181}$) form a contiguous concave surface surrounding Ser$^{52a}$ within CDR2β (Fig. 4*B*). Like TSST-1, the hot regions from either SpeC or hVβ2.1 are perfectly juxtaposed within the SpeC-Vβ2.1 interface (Fig. 4*B*) and taken together demonstrates that the non-canonical conformation of the CDR2β loop is the critical determinant for the molecular recognition of hVβ2 by SpeC.

*CDR2β Contacts Determine Vβ Specificity for Group V SAgs*—Existing structural information indicates that despite divergent binding architectures, all bacterial SAgs engage the CDR2β of their respective Vβ ligand (Fig. 1) (9, 39). We have shown that CDR2β contributes disproportionately in terms of functionality to form complexes with the Group I SAg TSST-1 and the Group IV SAg SpeC and prior biochemical studies have also confirmed that CDR2β loop contributes disproportionately in terms of energetics to form complexes with the Group II SAg SEC3 (40). In the absence of co-crystal structures for Group III SAgs in complex with Vβ, no such conclusions can be drawn for this SAg subset.

Because the CDR2β loop is critical for activation by Group I, II, and IV SAgs, we evaluated the role of CDR2β for Vβ-specificity in Group V SAgs. SEK and SpeI are both homologous Group V SAgs that show divergent Vβ-specificity. SpeI expands T cells with TCRs bearing hVβ6.7, hVβ9, and hVβ21 (8), while SEK almost exclusively targets T cells expressing hVβ5.1 (41). Recent crystallographic data for SEK with human hVβ5.1 showed that this subclass of SAg are unique be-

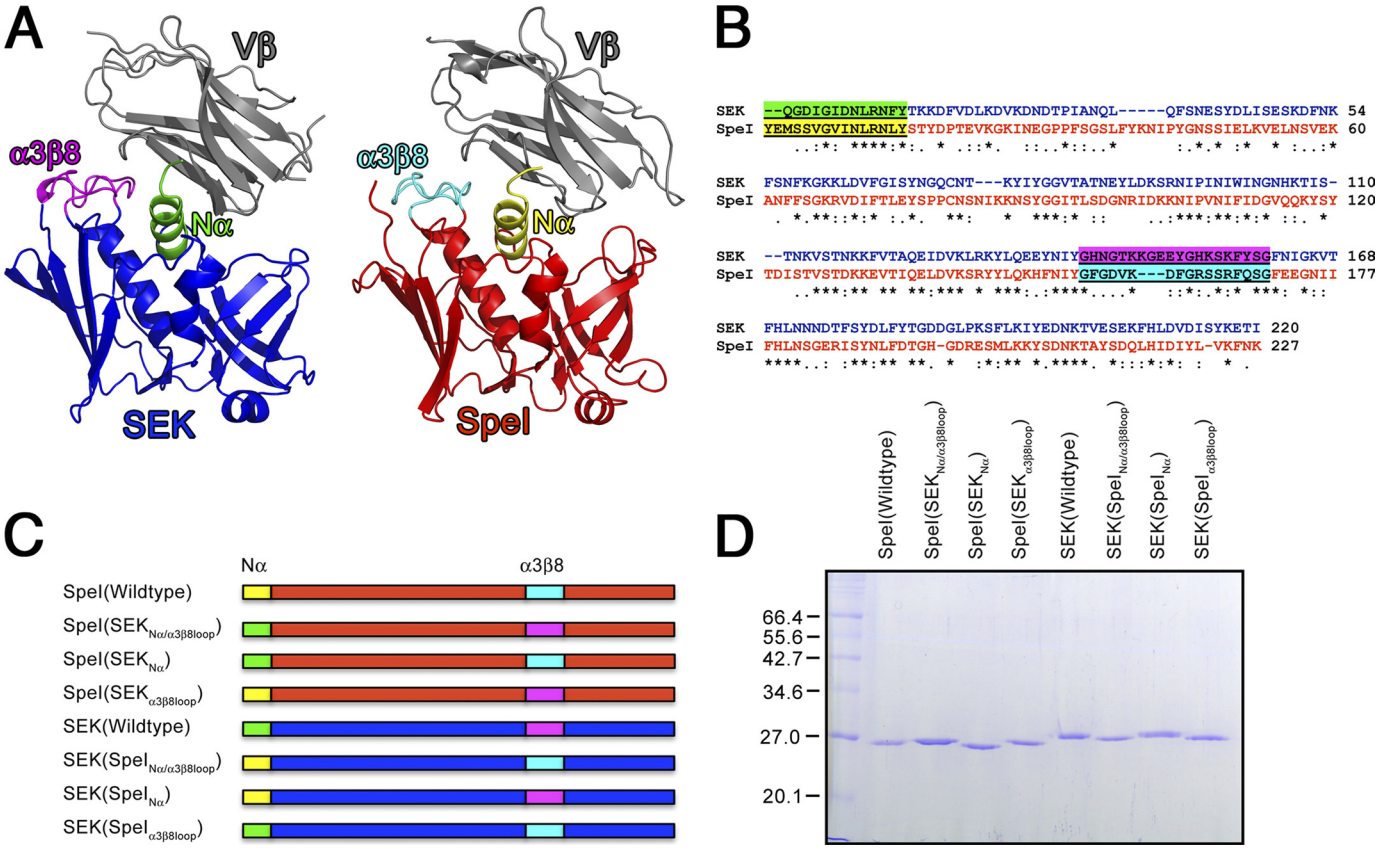


FIGURE 5. **Group V SAgs interact with their Vβ ligand through two distinct domains.** *A*, cartoon representations of two homologous Group V SAgs interacting with their Vβ ligand. Both SEK and SpeI interact with the CDR2β loop with their Nα domain, and with the FR3/4β regions with α3-β8 loop. Colors are as follows: Vβ domain, *gray*; SEK, *blue*; SpeI, *red*; SEK Nα domain, *green*; SEK α3-β8 loop, *magenta*; SpeI Nα domain, *yellow*, and SpeI α3-β8 loop, *cyan*. *B*, amino acid sequence alignment of SEK and SpeI showing the Nα domain and α3-β8 loop sequences used in the domain-swapping mutants. *C*, graphic representations of the domain swapping mutants colored coded as in *panel A*. *D*, SDS-PAGE of the purified the wild-type SpeI and SEK or hybrid proteins.

cause the intermolecular contacts with Vβ utilize distinct SAg domains to engage CDR2β and FR3/4β regions (18). The N-terminal α-helix of SEK (herein referred to as Nα) makes a number of contacts with the CDR2β loop, while the SEK α3-β8 loop makes contacts with both FR3β and FR4β regions (Fig. 5, *A* and *B*). To test which combination of these distinct binding domains where responsible for specific Vβ recognition, we constructed domain-swapped mutants of the N-terminal α-helix and the α3/β8 loop for SpeI and SEK with all possible combinations (Fig. 5, *C* and *D*). We used qRT-PCR to compare mature Vβ transcripts for hVβ5, hVβ6.7, hVβ9, and hVβ21 expressed from primary human lymphocytes activated with the various SAg hybrids. As predicted, wild-type SEK resulted in increased expression of hVβ5 transcripts relative to SpeI, while wild-type SpeI resulted in increased expression of hVβ6.7, hVβ9, and hVβ21 transcripts relative to SEK (Fig. 6). Remarkably, swapping of the CDR2β targeting N-terminal α-helix completely reversed this pattern for all tested Vβs such that the recombinant SAgs containing the SpeI Nα all resembled the Vβ-skewing pattern for SpeI, while recombinant SAgs containing the SEK Nα all resembled the Vβ-skewing pattern for SEK (Fig. 6). Although the α3/β8 loop did not affect hybrid reactivity to Vβ5 expressing T cells, it was apparent that the SEK α3/β8 loop was more efficient for the activation of human T cells expressing Vβ6.7 or 9. In these cases, the inclusion of both the Nα and α3-β8 loop domains from SpeI grafted onto SEK resulted in fewer transcripts compared with Nα alone. These differences can be explained by sequence comparisons within the α3-β8 loops and the Vβ FR4 sequences. SEK $His^{142}$ and $Tyr^{158}$ are known to be individually necessary for T cell activation of hVβ5.1 expressing T cells (18) and the corresponding residues in SpeI are $Phe^{155}$ and $Gln^{168}$, respectively (8). SEK $His^{142}$ hydrogen bonds with $Ser^{63}$ in FR3β, a residue conserved in all four analyzed Vβs. SEK $His^{142}$ also hydrogen bonds with hVβ5.1 $Asn^{75}$, and SEK $Tyr^{158}$ hydrogen bonds to hVβ5.1 $Thr^{78}$. These FR4β residues are polymorphic between the different Vβs, thus either individually or in combination the SpeI α3-β8 loop residues are less efficient for engaging FR4β. Thus, although the FR3/4β contacts influence the magnitude of the response, this data establishes that CDR2β is the critical determinant for Vβ selectivity by Group V SAgs.

*CDR2β as the Universal SAg Target*—The current understanding of SAgs with promiscuous Vβ profiles is that these toxins interact primarily with main-chain atoms of Vβs, and thus Vβ discrimination is more dependent on overall CDR conformation, rather than specific amino acid side chains. SEB and SEC3 are two such promiscuous SAgs and the crystal structure of their common ligand, mouse Vβ8.2 (mVβ8.2)-chain, has been solved unbound and in complex with two different pMHC II complexes (42), as well as in complex with SEC3 (6) and SEB (19). SEC3 and SEB interact primarily with the CDR2β and HV4β loops of mVβ8.2 and superposition of

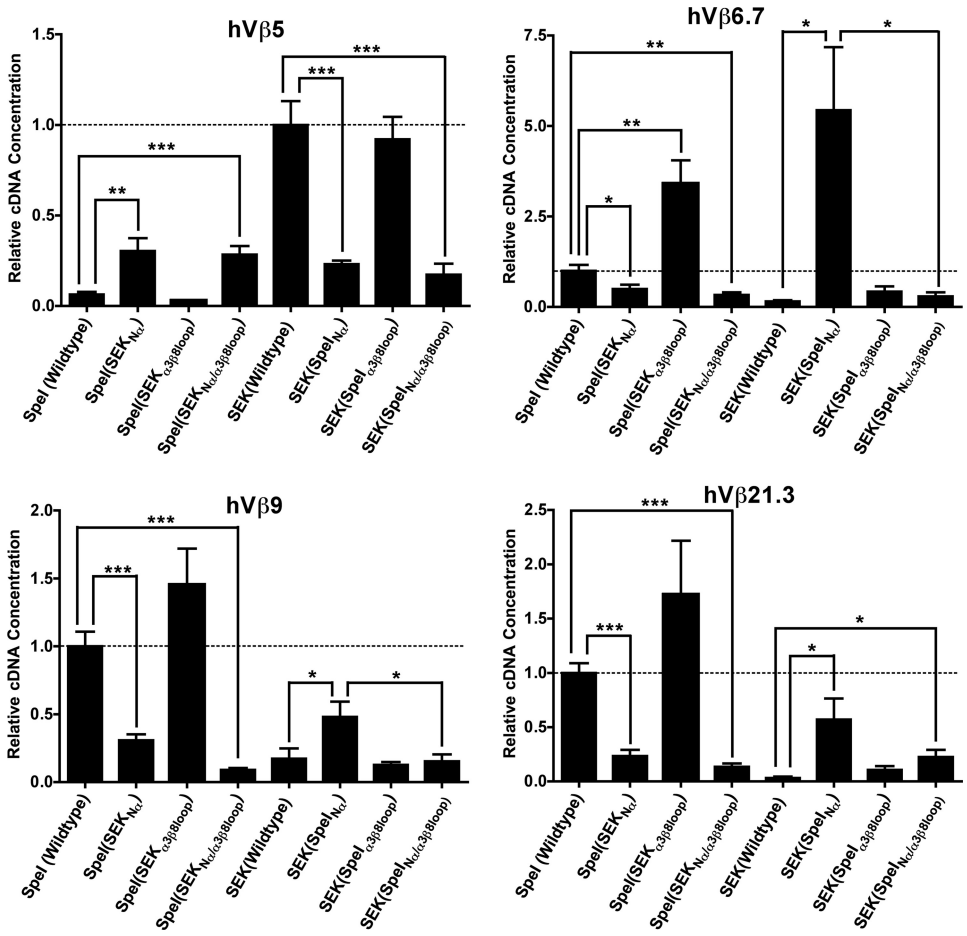


FIGURE 6. **The N-terminal α-helix (Nα) domain of Group V SAgs governs Vβ specificity through contacts with CDR2β.** qRT-PCR analysis of Vβ expression from human PBMC stimulated with 1 μg/ml of the wild-type SpeI and SEK or hybrid proteins shown in Fig. 5*D*. The data were normalized and set at 1.0 (*dashed line*) to responses from the wild-type SAg for the corresponding Vβ target (SpeI targets hVβ6.7, 9 and 21.3 while SEK targets hVβ5). Data are the average ± S.E. from three independent donors each done in triplicate ($n = 9$). Statistical significance was determined between the values from wild-type SAg and corresponding domain-swapped mutants, and values between the Nα domain-swapped mutants and the double Nα/α3β8 loop-swapped mutants (*, $p < 0.05$; **, $p < 0.01$; and ***, $p < 0.001$).

the CDR1β, CDR2β, and HV4β loops from the various mVβ8.2 structures reveals that there are minimal movements of the CDR1β, CDR2β, and HV4β loops when in complex with SEB, SEC3, and pMHC II, in comparison to the unbound structure. Hence SEC3 and SEB bind to Vβs with similar architectures in a lock and key fashion. However, superposition of the crystal structures of Vβ2.1 in complex with TSST-1, SpeC (21) and pMHC II (43) shows the CDR2β loop undergoes significant conformational changes upon SAg binding. Assuming that the conformation of CDR2β in complex with pMHC is similar to the unbound state, as in other TCR-pMHC complexes (42, 44, 45), the CDR2β loop is pushed away from its native state by both TSST-1 and SpeC. Hence the molecular basis for the Vβ specificity of both TSST-1 and SpeC, similar to the more promiscuous SAgs, is also primarily driven by conformational recognition of CDR2β, but is also coupled to plasticity of CDR2β.

Collectively, this information reveals that although there are Vβ residues that are individually essential for the generation of functional SAg-mediated T cell activation complexes, molecular recognition by both TSST-1 and SpeC is driven primarily not by sequence dependence of CDR2β, but similar to the more promiscuous SAgs, by conformational recognition of CDR2β. This provides new insight into the molecular basis of Vβ targeting by highly specific bacterial SAgs. In addition, the domain swapping experiments establish that, at least for the Group V SAgs, that the CDR2β contacts allow SAgs to discriminate between different Vβs.

Analysis of multiple TCR-pMHC complexes with the same Vβ-chain has shown that differences in CDR3β sequence did not influence MHC footprints on the TCRs. Rather, germ line encoded regions of TCR and MHC, so called Vβ structural codons, influence rotational orientations implying the Vβ domain plays a critical role in TCR-based recognition (42, 46). It seems that bacterial SAgs have evolved to target an intrinsic structural feature of the TCR, imposed by the MHC molecule, critical for the specific recognition and activation of T cells.

## REFERENCES

1. Garcia, K. C., Teyton, L., and Wilson, I. A. (1999) *Annu. Rev. Immunol.* **17,** 369–397
2. Garcia, K. C., and Adams, E. J. (2005) *Cell* **122,** 333–336
3. Norton, S. D., Schlievert, P. M., Novick, R. P., and Jenkins, M. K. (1990)

*J. Immunol.* **144,** 2089–2095
4. Mollick, J. A., Cook, R. G., and Rich, R. R. (1989) *Science* **244,** 817–820
5. White, J., Herman, A., Pullen, A. M., Kubo, R., Kappler, J. W., and Marrack, P. (1989) *Cell* **56,** 27–35
6. Fields, B. A., Malchiodi, E. L., Li, H., Ysern, X., Stauffacher, C. V., Schlievert, P. M., Karjalainen, K., and Mariuzza, R. A. (1996) *Nature* **384,** 188–192
7. McCormick, J. K., Yarwood, J. M., and Schlievert, P. M. (2001) *Annu. Rev. Microbiol.* **55,** 77–104
8. Brouillard, J. N., Günther, S., Varma, A. K., Gryski, I., Herfst, C. A., Rahman, A. K., Leung, D. Y., Schlievert, P. M., Madrenas, J., Sundberg, E. J., and McCormick, J. K. (2007) *J. Mol. Biol.* **367,** 925–934
9. Sundberg, E. J., Deng, L., and Mariuzza, R. A. (2007) *Semin Immunol.* **19,** 262–271
10. Jardetzky, T. S., Brown, J. H., Gorga, J. C., Stern, L. J., Urban, R. G., Chi, Y. I., Stauffacher, C., Strominger, J. L., and Wiley, D. C. (1994) *Nature* **368,** 711–718
11. Kasper, K. J., Xi, W., Nur-Ur, Rahman, A. K., Nooh, M. M., Kotb, M., Sundberg, E. J., Madrenas, J., and McCormick, J. K. (2008) *J. Immunol.* **181,** 3384–3392
12. Kim, J., Urban, R. G., Strominger, J. L., and Wiley, D. C. (1994) *Science* **266,** 1870–1874
13. Lavoie, P. M., McGrath, H., Shoukry, N. H., Cazenave, P. A., Sékaly, R. P., and Thibodeau, J. (2001) *J. Immunol.* **166,** 7229–7237
14. Papageorgiou, A. C., Acharya, K. R., Shapiro, R., Passalacqua, E. F., Brehm, R. D., and Tranter, H. S. (1995) *Structure* **3,** 769–779
15. Petersson, K., Håkansson, M., Nilsson, H., Forsberg, G., Svensson, L. A., Liljas, A., and Walse, B. (2001) *EMBO J.* **20,** 3306–3312
16. Li, Y., Li, H., Dimasi, N., McCormick, J. K., Martin, R., Schuck, P., Schlievert, P. M., and Mariuzza, R. A. (2001) *Immunity* **14,** 93–104
17. Andersen, P. S., Schuck, P., Sundberg, E. J., Geisler, C., Karjalainen, K., and Mariuzza, R. A. (2002) *Biochemistry* **41,** 5177–5184
18. Günther, S., Varma, A. K., Moza, B., Kasper, K. J., Wyatt, A. W., Zhu, P., Rahman, A. K., Li, Y., Mariuzza, R. A., McCormick, J. K., and Sundberg, E. J. (2007) *J. Mol. Biol.* **371,** 210–221
19. Li, H., Llera, A., Tsuchiya, D., Leder, L., Ysern, X., Schlievert, P. M., Karjalainen, K., and Mariuzza, R. A. (1998) *Immunity* **9,** 807–816
20. Moza, B., Varma, A. K., Buonpane, R. A., Zhu, P., Herfst, C. A., Nicholson, M. J., Wilbuer, A. K., Seth, N. P., Wucherpfennig, K. W., McCormick, J. K., Kranz, D. M., and Sundberg, E. J. (2007) *EMBO J.* **26,** 1187–1197
21. Sundberg, E. J., Li, H., Llera, A. S., McCormick, J. K., Tormo, J., Schlievert, P. M., Karjalainen, K., and Mariuzza, R. A. (2002) *Structure* **10,** 687–699
22. Wang, L., Zhao, Y., Li, Z., Guo, Y., Jones, L. L., Kranz, D. M., Mourad, W., and Li, H. (2007) *Nat. Struct. Mol. Biol.* **14,** 169–171
23. Reichmann, D., Rahat, O., Albeck, S., Meged, R., Dym, O., and Schreiber, G. (2005) *Proc. Natl. Acad. Sci. U.S.A.* **102,** 57–62
24. Keskin, O., Ma, B., and Nussinov, R. (2005) *J. Mol. Biol.* **345,** 1281–1294
25. Moza, B., Buonpane, R. A., Zhu, P., Herfst, C. A., Rahman, A. K., McCormick, J. K., Kranz, D. M., and Sundberg, E. J. (2006) *Proc. Natl. Acad. Sci. U.S.A.* **103,** 9867–9872
26. Rahman, A. K., Herfst, C. A., Moza, B., Shames, S. R., Chau, L. A., Bueno, C., Madrenas, J., Sundberg, E. J., and McCormick, J. K. (2006) *J. Immunol.* **177,** 8595–8603
27. Li, P. L., Tiedemann, R. E., Moffat, S. L., and Fraser, J. D. (1997) *J. Exp. Med.* **186,** 375–383
28. Marrack, P., and Kappler, J. (1990) *Science* **248,** 1066
29. Sambrook, J., and Russell, D. W. (2001) *Molecular Cloning: A Laboratory Manual*, 3 rd Ed., Cold Spring Harbor Laboratory Press, Cold Spring Harbor, NY
30. Gootenberg, J. E., Ruscetti, F. W., Mier, J. W., Gazdar, A., and Gallo, R. C. (1981) *J. Exp. Med.* **154,** 1403–1418
31. Choi, Y. W., Kotzin, B., Herron, L., Callahan, J., Marrack, P., and Kappler, J. (1989) *Proc. Natl. Acad. Sci. U.S.A.* **86,** 8941–8945
32. Buonpane, R. A., Moza, B., Sundberg, E. J., and Kranz, D. M. (2005) *J. Mol. Biol.* **353,** 308–321
33. McCormick, J. K., Tripp, T. J., Llera, A. S., Sundberg, E. J., Dinges, M. M., Mariuzza, R. A., and Schlievert, P. M. (2003) *J. Immunol.* **171,** 1385–1392
34. Tripp, T. J., McCormick, J. K., Webb, J. M., and Schlievert, P. M. (2003) *Infect. Immun.* **71,** 1548–1550
35. Hurley, J. M., Shimonkevitz, R., Hanagan, A., Enney, K., Boen, E., Malmstrom, S., Kotzin, B. L., and Matsumura, M. (1995) *J. Exp. Med.* **181,** 2229–2235
36. Hennecke, J., Carfi, A., and Wiley, D. C. (2000) *EMBO J.* **19,** 5611–5624
37. Gazdar, A. F., Carney, D. N., Bunn, P. A., Russell, E. K., Jaffe, E. S., Schechter, G. P., and Guccion, J. G. (1980) *Blood* **55,** 409–417
38. Gluschankof, P., and Suzan, M. (2002) *Virology* **300,** 160–169
39. Sundberg, E. J. (2009) *Methods Mol. Biol.* **524,** 347–359
40. Churchill, H. R., Andersen, P. S., Parke, E. A., Mariuzza, R. A., and Kranz, D. M. (2000) *J. Exp. Med.* **191,** 835–846
41. Orwin, P. M., Leung, D. Y., Donahue, H. L., Novick, R. P., and Schlievert, P. M. (2001) *Infect. Immun.* **69,** 360–366
42. Feng, D., Bond, C. J., Ely, L. K., Maynard, J., and Garcia, K. C. (2007) *Nat. Immunol.* **8,** 975–983
43. Hahn, M., Nicholson, M. J., Pyrdol, J., and Wucherpfennig, K. W. (2005) *Nat. Immunol.* **6,** 490–496
44. Ishizuka, J., Stewart-Jones, G. B., van der Merwe, A., Bell, J. I., McMichael, A. J., and Jones, E. Y. (2008) *Immunity* **28,** 171–182
45. Wu, L. C., Tuot, D. S., Lyons, D. S., Garcia, K. C., and Davis, M. M. (2002) *Nature* **418,** 552–556
46. Garcia, K. C., Adams, J. J., Feng, D., and Ely, L. K. (2009) *Nat. Immunol.* **10,** 143–147
47. Thompson, J. D., Higgins, D. G., and Gibson, T. J. (1994) *Nucleic Acids Res.* **22,** 4673–4680